January 2014

Digital fringe profilometry based on triangular fringe patterns and spatial shift estimation

Pu Cao
University of Wollongong, pc241@uowmail.edu.au

Jiangtao Xi
University of Wollongong, jiangtao@uow.edu.au

Yanguang Yu
University of Wollongong, yanguang@uow.edu.au

Qinghua Guo
University of Wollongong, qguo@uow.edu.au

Digital fringe profilometry based on triangular fringe patterns and spatial shift estimation

Abstract

In this paper, we present a new approach for the 3D measurement using digital fringe projection. Instead of sinusoidal fringe patterns and the traditional phase shift detection, the proposed technique makes use of triangular patterns and the spatial shift estimation for extract the 3D shape. The proposed technique is advantageous not only by improved immunization to nonlinear distortion associated with digital projections, but also reduced computational burden for its implementation. Theoretical analysis and experimental results are also presented to confirm the effectiveness of the proposed technique.

Keywords

shift, spatial, patterns, triangular, profilometry, fringe, estimation, digital

Publication Details

P. Cao, J. Xi, Y. Yu & Q. Guo, "Digital fringe profilometry based on triangular fringe patterns and spatial shift estimation," in Proceedings of SPIE: Dimensional Optical Metrology and Inspection for Practical Applications III, 2014, pp. 91100C-1-91100C-15.

Digital Fringe Profilometry Based On Triangular Fringe Patterns and Spatial Shift Estimation

Pu Cao, Jiangtao Xi*, Yanguang Yu and Qinghua Guo
School of Electrical, Computer and Telecommunications Engineering
University of Wollongong, Wollongong, NSW2522, Australia

ABSTRACT

In this paper, we present a new approach for the 3D measurement using digital fringe projection. Instead of sinusoidal fringe patterns and the traditional phase shift detection, the proposed technique makes use of triangular patterns and the spatial shift estimation for extract the 3D shape. The proposed technique is advantageous not only by improved immunization to nonlinear distortion associated with digital projections, but also reduced computational burden for its implementation. Theoretical analysis and experimental results are also presented to confirm the effectiveness of the proposed technique.

Keywords: fringe pattern profilometry, 3D measurement, digital fringe projection

1. Introduction:

In recent years, optical noncontact three-dimension (3D) profile measurement has attracted increasing research efforts due to many potential applications. Among other approaches, the Fringe Pattern Profilometry (FPP) based on Digital Fringe Projection (DFP) has been proven to be one of the most promising techniques due to the advantages of simple system structure, flexible fringe pattern generation and high accuracy.

Figure 1 shows the system structure of a DFP based FPP, consisting of a digital video projector, a CCD camera and a reference plane. A frame of image with a particular fringe pattern produced by the digital projector is casted onto the reference plane, and then onto the surface of the object when the reference plane is removed. The light reflected from the reference plane and the object surface are captured by the CCD camera, with the later being a deformed version of the former due to the variance of the height of the object surface. The deformed fringe pattern carries the information of surface shape, and 3D profile of the object can be retrieved from the two fringe patterns.

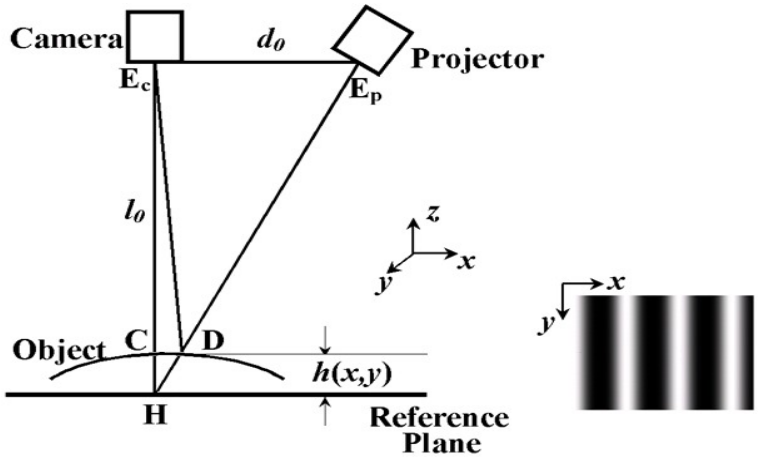

Figure 1. Schematic diagram of FPP system.

*jiangtao@uow.edu.au; phone 61 2 42213412; fax 61 2 42213236

Dimensional Optical Metrology and Inspection for Practical Applications III, edited by Kevin G. Harding, Toru Yoshizawa, Song Zhang, Proc. of SPIE Vol. 9110, 91100C

A number of FPP approaches have been introduced. The most widely used methods are on the basis of phase detection (PD) or phase difference detection (PDD) [1-6]. In these approaches, the deformed fringe pattern is considered as the result of phase modulation of the original fringe pattern, and hence detection of phase maps from original and deformed fringe patterns enables the retrieval of the 3D shape. However, PDD approaches also suffer from a number of disadvantages. A major problem is the influence of nonlinear distortions inherent to digital video projection [7, 8]. Such distortions make it difficult for the original fringe patterns to be either sinusoidal or ideal periodic, which are required by PDD based approaches. As an effort to solve the problem, Hu, et al. [9] proposed an approach referred to as Spatial Shift Estimation (SSE) profilometry, which instead of detecting the phase difference between the phase maps, is based on the estimation of spatial shift for corresponding pixels on the two fringe patterns.

Compared to PDD based approaches, SSE techniques are advantageous in that non-sinusoidal fringe patterns can be employed, and that they do not suffer from the nonlinear distortion associated with the digital fringe projection. However, these advantages are not fully exploited, as the fringe patterns are usually sinusoidal in the existing work on SSE [9, 10, 11]. Although the influence of nonlinear distortions can be remedied, computational burden associated with the reported work on SSE is still rather heavy.

In this paper, we will investigate the use of non-sinusoidal fringe patterns with the aim to improve the efficiency in terms of computation. In particular, we propose to employ triangular patterns which will lead to significant reduction in computation burden in contrast to other commonly used ones, such as sinusoidal fringe patterns.

This paper is organized as follows. In Section 2 we firstly present a brief description of conventional PDD and SSE based FPP, including working principles, system structures and relevant algorithms. Shortcomings and limitation associated with the use of sinusoidal fringe patterns are discussed in Section 3. In Section 4 we introduce a triangular fringe pattern instead of sinusoidal based on theoretic analysis. Experiment results are presented in Section 5 which to verify the effectiveness and advantages of the triangular fringe patterns. Section 6 concludes the paper.

2. Problem Statement

2.1. Principle of Triangulation

Operation of FPP is based on the triangulation principle described as follows. As the image projected has a fringe structure, without loss of generality we assume that light intensity varies periodically alone x direction, while keeping constant along y direction, as shown in Figure 1. Hence we can use $s(x)$ and $d(x)$ to denote the variance of light intensity of the fringe pattern on the reference plane and object surface respectively. We will use $h(x)$ to denote the height distribution of the object surface along x-coordinate. We also assume that the reference plane and the object surface have the same reflective characteristics.

Let us consider what happens when a beam of light is projected onto the point D on the object. From Figure 1, we can see when the object is removed, the same light beam (hence with the same intensity) should be projected onto point H on the reference surface, which is reflected back to the camera through point C. As the triangles $E_c E_P H$ and CDH are similar, we are able to obtain the following relationship to determine the height of object at x_d:

$$h(x_d) = \frac{l_0 \overline{CD}}{d_0} \tag{1}$$

Note that x_d denotes the coordination of point D. $h(x_d)$ denotes the distance between points C and the reference plane. $\overline{CD}$ is the distance between points C and D. The above relationship is the foundation for FPP.

2.2. PDD-based Profilometry

Phase Difference Detection (PDD) is a class of widely used approaches for FPP. With PDD, the fringe patterns projected are sinusoidal or periodic, which can be expressed as follows [1, 2]:

$$s(x) = \sum_{k=0}^{+\infty} b_k \cos(2\pi k f_0 x + \psi_k) \tag{2}$$

and the deformed fringe pattern reflected from the object surface is:

$$d(x) = \sum_{k=0}^{+\infty} b_k \cos(2\pi k f_0 x + \phi_k(x) + \psi_k) \tag{3}$$

In the above expressions, f_0 is the spatial frequency of the fundamental component in the fringe patterns, and b_k is the amplitude of the k-th order harmonic component. ψ_k is the initial phase of the k-th order harmonic component. $\phi_k(x)$ denotes the phase difference between the k-th order harmonic components of these two fringe patterns, that is, the phase shift between C and D can be determined by the spatial distance $\overline{CD}$, that is [1, 2]:

$$\phi_k(x) = 2\pi k f_0 \overline{CD} = k \cdot 2\pi f_0 \overline{CD} = k \cdot \phi(x) \tag{4}$$

where $\phi(x) = 2\pi f_0 \overline{CD}$ is the phase shift of the fundamental component.

Substituting Equation (4) to Equation (1) we have:

$$h(x) = \frac{l_0 \phi(x)}{2\pi f_0 d_0} \tag{5}$$

Equation (5) shows that as long as $\phi(x)$ can be detected, we are able to calculate the height distribution $h(x)$ of the object surface. This is the foundation of all PDD based approaches.

A number of fringe pattern analysis methods have been developed to detect $\phi(x)$, such as Fourier Transform Profilometry (FTP) [3], Phase Shifting Profilometry (PSP), Phase Measuring Profilometry (PMP) [4, 5, 6], Modulation Measurement Profilometry (MMP) [12], Spatial Phase Detection (SPD) [13, 14], Phase Lock Loop (PLL) profilometry [15], Moiré Technique (MT) [16], colour-coded fringe projection [17, 18] and other methods [19, 20].

2.3. Nonlinear Distortions associated with Digital Projection

As mentioned above, all PDD based approaches require projection of sinusoidal or periodic fringe patterns. However, in practice, it is hard to meet this requirement due to the undesired factors inherent to digital projection. A major problem is the nonlinear projection luminous response, referred to as Gamma distortion [7, 8], which is introduced by visual display systems in order to enhance human perception of the sensation of lightness. The distortion can be modelled as follows [7, 8]:

$$w(x) = v(x)^{\gamma} \qquad \text{for} \qquad u \in [0,1] \tag{6}$$

where $v(x)$ is the image intensity function delivered to projector, and $w(x)$ is the actual output image intensity distribution. γ is a fractional number within $1 < \gamma < 3$. Obviously, even if a pure sinusoidal fringe pattern is delivered to the projector, the resulting one will no longer be a sinusoidal due the influence of Gamma distortion.

In order to overcome the nonlinear distortion, a number of methods have been proposed. Guo, *et al.* [21] proposed a method which approximates the gamma value using iterative statistical analysis of digital fringe patterns. However, it does not work if the single parameter model in Eq. (6) is not able to accurately describe the distortion, which always happens in practice. Baker, *et al.* [8] introduced a defocus method to deal the gamma distortion, where the high order harmonic waveforms are filtered out by means of defocusing the projector thus no additional computation for correction or compensation is required. However, the requirement to adjust parameter for gamma modeling and defocusing is complex. Zhang, *et al.* [22] also proposed a phase error compensation method by using a lookup table (LUT) to store and compensate the phase error. This method does not employ a mathematical model, which is suitable for non-analytical situations. However, the result of this compensation method is unstable since it only computes the gamma at center of projected image. The accuracy of the method is depended by the length of LUT. Hence it is time-consuming for high accuracy compensation. Zhang and Yau [23] then presented another LUT-based method which requires no pre-computing of the gamma. However, the accuracy of the results is still depends on the length of LUT. Pan, *et al.* [24] introduced an iterative phase compensation algorithm based on the theoretical analysis of the phase error. This method works well for gamma compensation, but it is vulnerable to the influence caused by other factors, such as background brightness and reflectivity of reference plane. Liu, *et al.* [25] developed a complicated gamma model to increase the accuracy of compensation, while the computing time is also increased.

2.4. SSE-based Profilometry

As an effort to combat the distortion problem, Hu, *et al*. proposed a class of approaches called Spatial Shift Estimation (SSE) profilometry [9]. The idea of SSE based approaches is rather simple and straight forward. Let us look at Figure 1 again. As x_d and x_c are the points on $d(x)$ and $s(x)$ with the same light intensity, that is $d(x_d) = s(x_c)$, we have:

$$d(x_d) = s(x_d - u(x_d)) \tag{7}$$

where $u(x_d) = \overline{CD} = x_d - x_c$, which is the spatial shift between x_d and x_c. As the above derivation is valid for all values of x_d and x_c, x_d can be replaced by x, yielding the following:

$$d(x) = s(x - u(x)) \tag{8}$$

Hence Eq. (1) can be expressed as:

$$h(x) = \frac{l_0 u(x)}{d_0} \tag{9}$$

Equations (8) and (9) provide a straight forward way to measure the 3D profile of the object surface. For every pixel on $d(x)$, we will locate the corresponding pixel on $s(x)$ with the same intensity (i.e. $d(x) = s(x - u(x))$), and then we work out the spatial distance between the two points (i.e., $u(x)$). The height of the object at the location of *x* can be determined by Equation (9). By repeating the procedure for all pixels on $d(x)$ (including all the *y* values), 3D profile of the object surface can be obtained.

At discussed above, the key to reconstruct object surface using SSE is to obtain the shift distribution $u(x)$ from $d(x)$ and $s(x)$. A number of approaches were proposed to achieve this [9, 10, 11]. Among these approaches, the one referred to as Inverse Function based Shift Estimation (IFSE) [11] is particularly interesting and briefed as follows. For a monotonic segment of $s(x)$, there exists a function which is unique and the inverse function of $s(x)$, that is:

$$s^{-1}\left[s(x)\right] = x \tag{10}$$

Applying this inverse function $s^{-1}(v)$ to the deformed signal $d(x)$, we have:

$$s^{-1}(d(x)) = s^{-1}\{s[x - u(x)]\} = x - u(x) \tag{11}$$

Hence the shift distribution function $u(x)$ can be retrieved by:

$$u(x) = x - s^{-1}(d(x)) \tag{12}$$

Now the key problem is to obtain the inverse function $s^{-1}(v)$. A simple way is to employ the polynomial curve fitting, that is, employing a polynomial function $f_k(v)$ to approximate $s^{-1}(v)$. As $s^{-1}\left[s(x)\right] = x$, $f_k(v)$ can be determined by minimization of the following average square error (i.e., the curve fitting error):

$$e_k = \frac{1}{N}\sum_{i=1}^{N}[(f_k(s(x_i)) - x_i)^2] \tag{13}$$

where N is the number of data samples, $f_k(v)$ is the polynomial of order k, that is, $f_k(v) = a_k v^k + a_{k-1} v^{k-1} + \ldots + a_1 v + a_0$. The accuracy of the above estimation depends on k and the characteristic of the inverse function, which then depends on that of $s(x)$.

The above spatial shift based approach has a great advantage. The projected fringe patterns are no longer required to be sinusoidal or periodic, leading to an increased freedom for the selection of the fringe patterns. Also, the approach does not suffer from the influence of nonlinear distortion.

3. Limitations of sinusoidal fringe patterns for SSE-based profilometry

Although SSE approaches provide more degrees of freedom in fringe pattern selection, in the existing work on SSE [9, 10, 11], sinusoidal fringe patterns are still employed. The issue of choosing fringe patterns with the aim to achieve best efficiency and accuracy performance has remained an open issue.

As a matter of fact, use of sinusoidal fringe pattern is never the best choice for IFSE based SSE approach. As described above a straight forward method to obtain the inverse function of $s(x)$ is data fitting by the following polynomial function of k-th order. The coefficients $a_0, a_1, \cdots, a_k$, by the least square principle, can be determined by solving the equation below:

$$\begin{bmatrix} N & \sum_{i=1}^{N} x_i & \cdots & \sum_{i=1}^{N} x_i^k \\ \sum_{i=1}^{N} x_i & \sum_{i=1}^{N} x_i^2 & \cdots & \sum_{i=1}^{N} x_i^{k+1} \\ \vdots & \vdots & & \vdots \\ \sum_{i=1}^{N} x_i^k & \sum_{i=1}^{N} x_i^{k+1} & \cdots & \sum_{i=1}^{N} x_i^{2k} \end{bmatrix} \begin{bmatrix} a_0 \\ a_1 \\ \vdots \\ a_k \end{bmatrix} = \begin{bmatrix} \sum_{i=1}^{N} y_i \\ \sum_{i=1}^{N} x_i y_i \\ \vdots \\ \sum_{i=1}^{N} x_i^k y_i \end{bmatrix} \tag{14}$$

where N is the number of data samples. From Equation (14), it is clear that with the increase of k, there will be a significant increase in computational burden. Hence in order to improve the efficiency in terms of computational burden, the polynomial should be as simple as possible, that is, its order as low as possible.

In order to show the how the order of the polynomial is related to the shape of the fringes, we studied the sinusoidal fringe, and Figure 2 shows the monotonic part of a sinusoidal function, where the length of this segment is 100 pixels. We performed the data fitting on its inverse function with different degrees of polynomial. Table 1 shows the relationship between the curve fitting error e_k and *k*, the degrees of polynomial used to fitting, which clearly show that the degree of the polynomial must be high enough to approximate the inverse function.

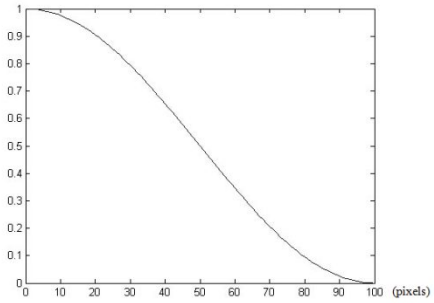

Figure 2. Selected monotonic interval of sinusoidal waveform

k	1	2	3	4	5
e_k	12.0773	12.0594	1.9247	1.9197	0.6070

k	6	7	8	9	10
e_k	0.6048	0.2633	0.2621	0.1373	0.1364

Table 1: curving fitting error in different polynomial degree

4. SSE-based profilometry using triangular fringe patterns

As analyzed above, sinusoidal fringe patterns are not the optimal choice for IFSE based SSE approach. Generally speaking, for a specific value of e_k, the more linear the inverse function $s^{-1}(v)$, the lower the order *k*. Hence we should choose the fringe pattern $s(x)$ in such a way that its inverse function is as linear as possible.

Based on this scenario we choose a triangular fringe pattern which is periodic and without loss of generality the light intensity within the first fringe period can be expressed as follows:

$$s(x)=\begin{cases} \dfrac{2a}{T_0}x, & when \quad 0\le x\le \dfrac{1}{2}T_0 \\ 2a\cdot(1-\dfrac{x}{T_0}), & when \quad \dfrac{1}{2}T_0\le x\le T_0 \end{cases} \tag{15}$$

where a is the contrast of the projected fringe, which is in the range of $[0,1]$. T_0 is the period of fringe. The whole image is a periodic extension of $s(x)$. Figure 3 shows an example of the pattern of 4 fringes with $a=1.0$ and $T_0=20$ pixels.

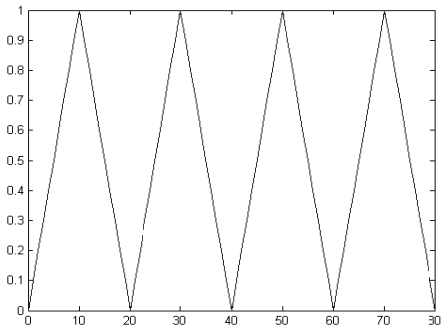

Figure 3. Triangle waveform

From Equation (15), it is seen the triangular function is linear and monotonic over every half of its period $nT_0 \le x \le (n+\frac{1}{2})T_0$ and $(n+\frac{1}{2})T_0 \le x \le (n+1)T_0$, where *n* is the fringe index. Obviously, such a linear function is very good as its inverse function is also a linear function. Considering $s(x)$ within the first fringe period, its inverse function is given by the following:

$$s^{-1}(v)=\begin{cases} \dfrac{T_0}{2a}v, & when \quad 0\le x\le \dfrac{1}{2}T_0 \\ T_0(1-\dfrac{v}{2a}), & when \quad \dfrac{1}{2}T_0\le x\le T_0 \end{cases} \tag{16}$$

The above relation implies that a linear function is sufficient to estimate the inverse function if there is no distortion associated with the projection. This is very advantageous as only two coefficients are required for a pure linear function. In the existence of nonlinear distortions, such triangular patterns still have great advantages, as the projected patterns are still close to linear, and so does the inverse function. Let us consider that the projected triangular fringe patterns are subject to Gamma distortion depicted by Equation (15). The actual projected pattern in the first fringe period as follows:

$$s(x)=\begin{cases} \left(\dfrac{2a}{T_0}\right)^{\gamma}x^{\gamma}, & when \quad 0\le x\le \dfrac{1}{2}T_0 \\ a^{\gamma}\cdot(2-\dfrac{2x}{T_0})^{\gamma}, & when \quad \dfrac{1}{2}T_0\le x\le T_0 \end{cases} \tag{17}$$

As γ is typically a fractional value within the range $1 < \gamma < 3$, it is easy to evaluate the minimal degree of the polynomial for it to approximate the inverse function with a given error. Figure 4 gives the results of numerical computation for the case when $\gamma = 2$. The x-axis is variable x, and y-axis is the results of $y = f_k\left[s(x)\right]$. When a perfect inverse function is employed, we should have $y = f_k\left[s(x)\right] = x$, which is the solid line. Using a 3rd order polynomial, the dashed line is obtained, which is very close to the solid line with a very small curve fitting error $e_k = 0.0231$. Hence a third order polynomial is enough to estimate the inverse function. In contrast, when sinusoidal fringe patterns are utilized, a 10th order polynomial is required to yield the same curve fitting error. Hence the triangular patterns are much better than the sinusoidal patterns.

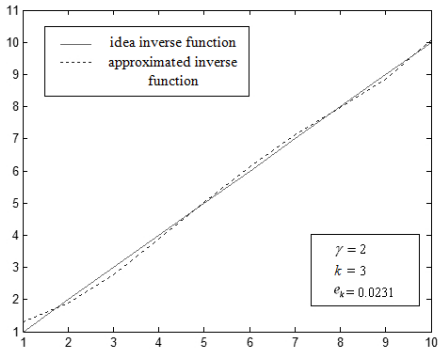

Figure 4. Curve of inverse functions

5. Simulation

In this section, simulation was employed to test the performance of the proposed triangular fringe pattern. A flat board with its height known as 10mm is simulated as the object surface. The fringe images were than distorted using gamma correction which the gamma value is set to 1.60.

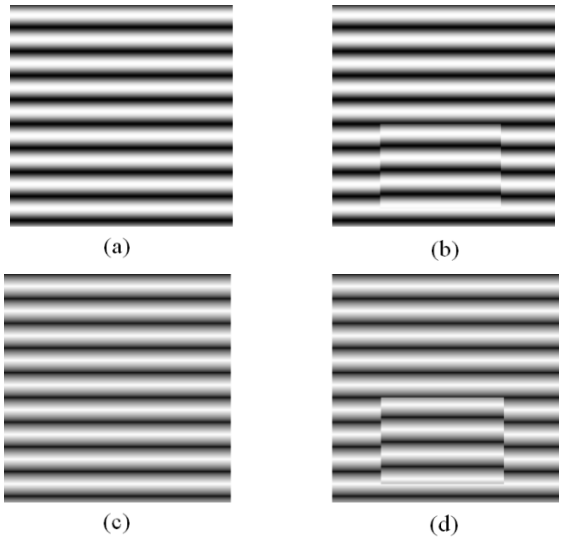

Figure 5. The simulated fringe images

Figure 5 gives the simulated fringe pattern images. Figures 5 (a) and (b) show the sinusoidal fringe pattern on the reference plane and on the object surface respectively, and Figures 5 (c) and (d) are using the triangular fringe pattern.

Figure 6 (a) shows the height distribution of cross section of the flat board at the central line. In these figure, *x* label stands for the length of flat board (in pixels), and *h* label is the height (mm). Note that the degree of the polynomial for

the inverse function is selected to be 3 (k=3). Figures 6 (b) and (c) show the results using sinusoidal fringe in the cases of k=3 and 10 respectively.

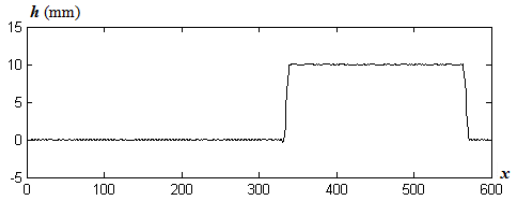

Retrieved Height Distribution using Triangular Fringe, k=3

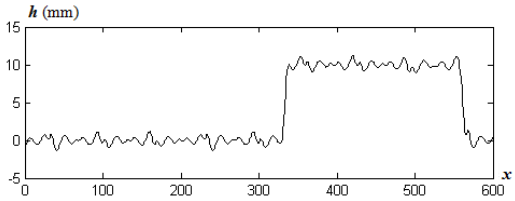

Retrieved Height Distribution using Sinusoidal Fringe, k=3

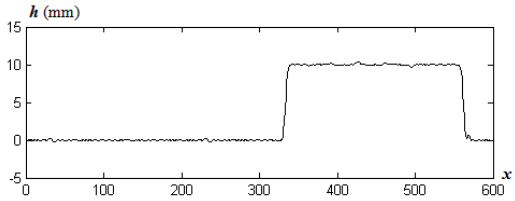

Retrieved Height Distribution using Sinusoidal Fringe, k=10

Figure 6. Retrieved height distribution result (simulated board)

The reconstructed 3D surface shape of the object is shown in Figure 7. Figure 7 (a) is the result using triangular fringe in the cases of k=3. The results which retrieved by using sinusoidal fringe with different polynomial degrees are also shown in Figures 7 (b) and (c) where the degrees are 3 and 10 respectively.

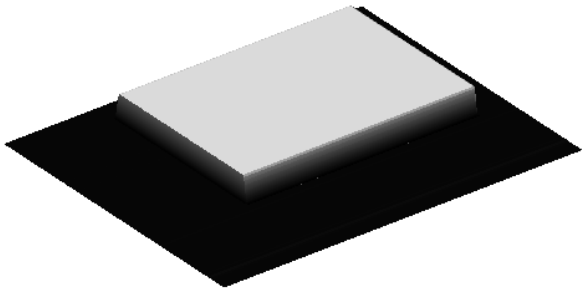

(a) 3D Reconstruct Result using Triangular Fringe, k=3

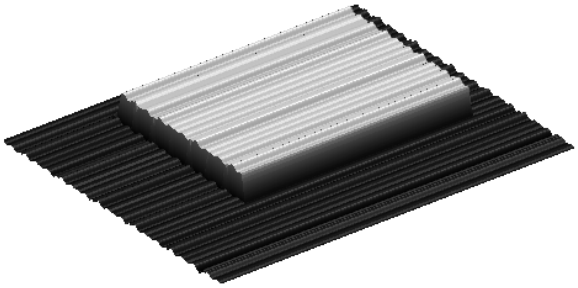

(b) 3D Reconstruct Result using Sinusoidal Fringe, k=3

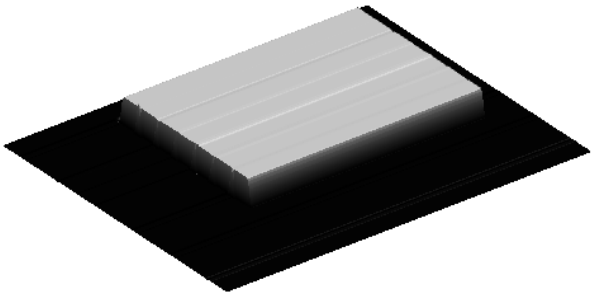

(c) 3D Reconstruct Result using Sinusoidal Fringe, k=10

Figure 7. 3D reconstruct results (simulated board)

The error distribution of these reconstruct results is also calculated and shown in table 2:

	Max Error (Positive)	Max Error (Negative)	Mean Square Error
Triangular Fringe (k=3)	0.0494mm	-0.0515mm	0.0007mm
Sinusoidal Fringe (k=3)	1.1923mm	-1.0033mm	0.2196mm
Sinusoidal Fringe (k=10)	0.3633mm	-0.3094mm	0.0084mm

Table 2: error distribution of reconstruct results (simulated board)

From the results above we can see that, with same polynomial degree, the triangular fringe performs much better than sinusoidal fringe. Also for the same level of accuracy, the degree of polynomial associated with triangular fringe patterns can be much lower than that with the sinusoidal patterns. The degree of the polynomial has significant impact on the efficiency of the 3D measurement in terms of computational burden and hence the time required. For the examples studied above where the degrees of the polynomials for sinusoidal and triangular patterns are 10 and 3 respectively, there will be a significant reduction in terms of computational burden with the proposed approach.

6. Experiments and Results

Experiments were also carried out in our laboratory to verify the validity of the proposed method. The experimental setup is shown in Figure 8. The digital projector used is HITACHI CP-X260, and camera is Duncan Tech MS3100. The digital camera is placed on top of the projector with a distance of 350 mm. The distance between the camera lens and the reference plan is 1295 mm.

The first object we used is a flat board where the height is 18mm. The resolution of the CCD camera is 1392×1039 pixels, and the field of vision for CCD camera is 250mm×187mm. Hence, the equivalent spatial resolution is 0.1796 mm/pixel.

Figure 8. The experimental system setup

The captured sinusoidal fringe patterns on the object surface and on the reference plane are shown in Figures 9 (a) and (b) respectively, and Figures 9 (c) and (d) are captured triangular fringe patterns on the object surface and on the reference plane. In the figure, we have 13 fringes, each covering 30 pixels.

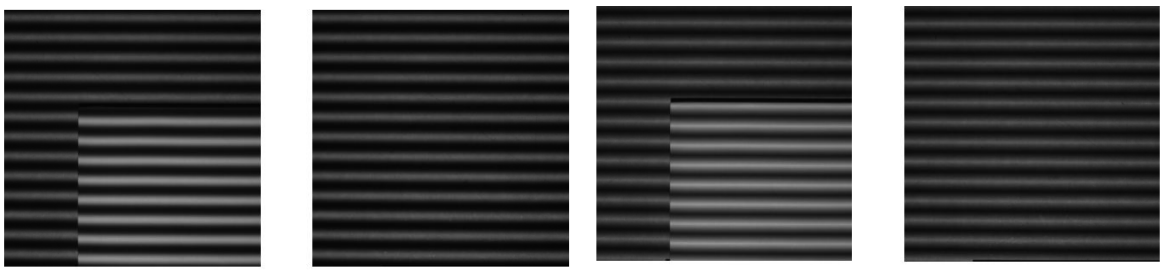

(a) (b) (c) (d)

Figure 9. Fringe patterns observed (board)

We divided the fringe into the monotonic intervals and applied IFSE approach to each of the intervals to obtain the height distribution of the board. Figure 10 (a) shows the height distribution of cross section of the board at the central line. In these figure, *x* label stands for the length of board (in pixels), and *h* label is the height (mm). Note that the degree of the polynomial for the inverse function is selected to be 3 (*k*=3).

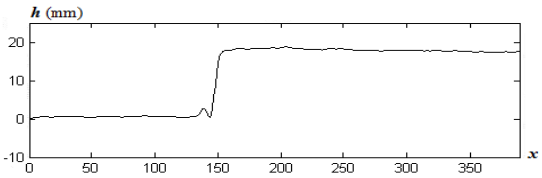

Retrieved Height Distribution using Triangular Fringe, k=3

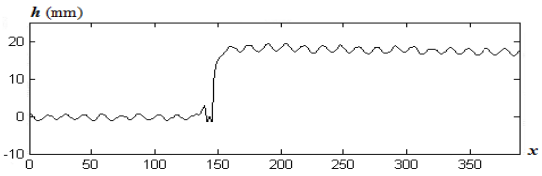

Retrieved Height Distribution using Sinusoidal Fringe, k=3

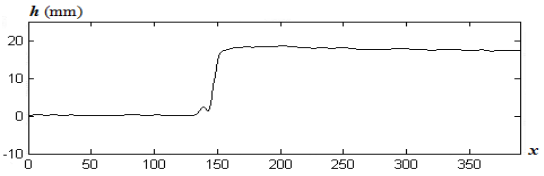

Retrieved Height Distribution using Sinusoidal Fringe, k=10

Figure 10. Retrieved height distribution result (board)

We also give the results of height distribution which retrieved by using sinusoidal fringe with different polynomial degrees. Figures 10 (b) and (c) show height distributions obtained for the cross section of the board, where the degree of the polynomials is 3 and 10 respectively.

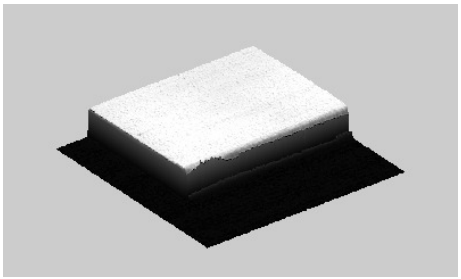

(a) 3D Reconstruct Result using Triangular Fringe, k=3

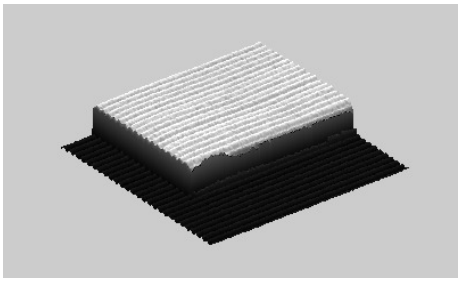

(b) 3D Reconstruct Result using Sinusoidal Fringe, k=3

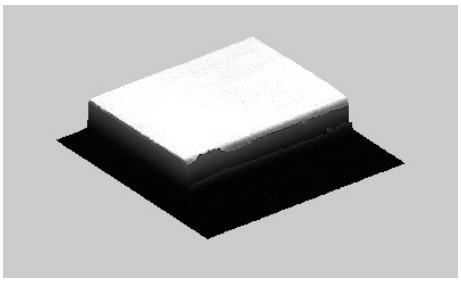

(c) 3D Reconstruct Result using Sinusoidal Fringe, k=10

Figure 11. 3D reconstruct results (board)

The 3D surface shape of the object is also reconstructed shown using triangular patterns as described above and the results are shown in Figure 11 (a) where the degree of polynomial is 3. For comparison, use of the sinusoidal patterns and polynomials of degree 3 and 10 are also depicted in Figures 11 (b) and (c). Since the height of this board is already known. The error distribution of these reconstruct results is calculated and shown in table 3:

	Max Error (Positive)	Max Error (Negative)	Mean Square Error
Triangular Fringe (k=3)	0.8290mm	-0.7094mm	0.1407mm
Sinusoidal Fringe (k=3)	1.4787mm	-2.0044mm	0.6493mm
Sinusoidal Fringe (k=10)	0.5456mm	-0.7875mm	0.1627mm

Table 3: error distribution of reconstruct results (board)

It can be seen that using polynomials with the same degree 3, the proposed triangular patterns yield much higher accuracy, while in order to achieve the same accuracy, the degree of the polynomial must be much higher (i.e. 10) in contrast to that used for triangular patterns (i.e., 3).

We also tested the proposed technique using another object which is a dome where the max height is 22.8mm. In this experiment, the digital camera is still placed on top of the projector with a distance of 350 mm. The distance between the camera lens and the reference plan is changed to 1195 mm. Figure 12 shows the captured fringe patterns using sinusoidal fringe pattern (a) and triangular fringe pattern (b). We have about 8 fringes, each covering 40 pixels.

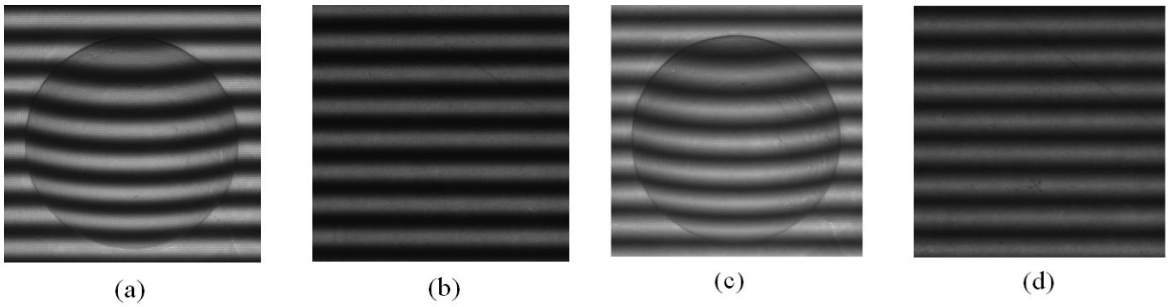

Figure 12. Fringe patterns observed (dome)

Figure 13 shows the height distribution obtained for the middle line in this dome. Figure 13 (a) is the result using triangular fringe pattern with polynomial degree k=3, and Figures 13 (b) and (c) gives the reconstructed object shape using sinusoidal fringe with polynomial degree k=3 and k=10 respectively. From these results, it can be seen that only the degree of polynomial equals to 10 or above, the employment of sinusoidal pattern can achieve the same accuracy as using triangular pattern with polynomial degree k=3.

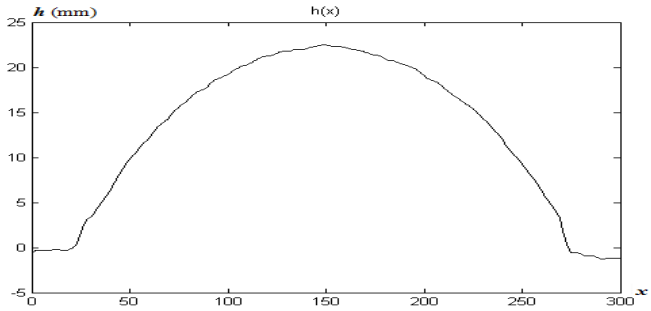

Retrieved Height Distribution using Triangular Fringe, k=3

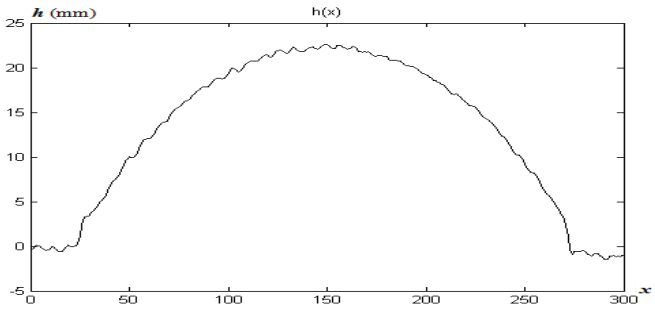

Retrieved Height Distribution using Sinusoidal Fringe, k=3

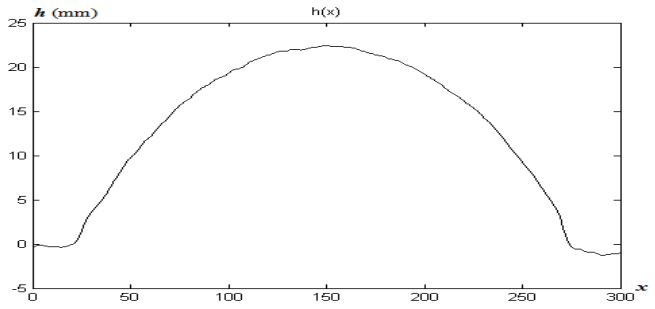

Retrieved Height Distribution using Sinusoidal Fringe, k=10

Figure 13. Retrieved height distribution result (dome)

Figure 14 gives the reconstructed 3D surface shape of the object. Figure 14 (a) is the result using triangular fringe in the cases of k=3. Figures 14 (b) and (c) show the results using sinusoidal fringe in the cases of k=3 and 10 respectively.

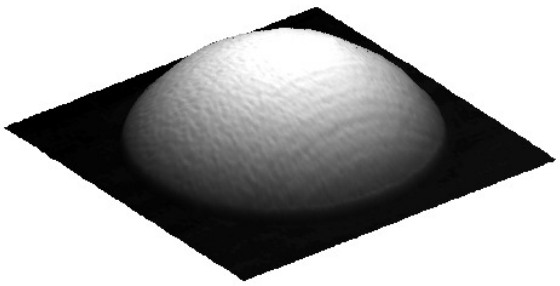

(a) 3D Reconstruct Result using Triangular Fringe, k=3

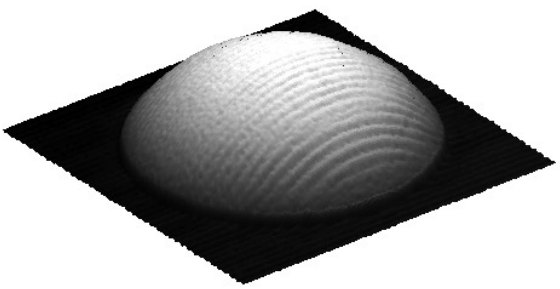

(b) 3D Reconstruct Result using Sinusoidal Fringe, k=3

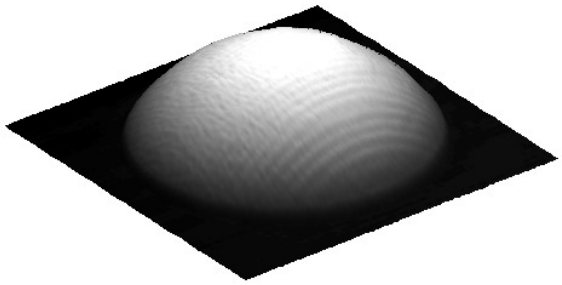

(c) 3D Reconstruct Result using Sinusoidal Fringe, k=10

Figure 14. 3D reconstruct results (dome)

From the results above we can still see the triangular fringe performs much better than sinusoidal fringe with same polynomial degree and for the same level of accuracy, the degree of polynomial associated with triangular fringe patterns can be much lower than that with the sinusoidal patterns. These experimental results successfully verified the efficiency of the proposed method.

7. Conclusion

In this paper, we demonstrated a new approach for implementing FPP, where the fringe patterns are triangular and the height distribution is calculated based on spatial shift estimation using inverse functions. In contrast to the phase detection based technique using sinusoidal fringe patterns, the proposed technique is advantageous by (1) better immunization to nonlinear distortions associated with digital projection, and (2) improved efficiency in terms of computational burden required for 3D measurement. The performance of the proposed technique has been verified by experiments.

It should be pointed out that the proposed approach is based on projection of a single fringe pattern, and the measurement accuracy is not as high as the approaches using multiple image patterns, such as phase shift profilometry (PSP). Also, the spatial shift is calculated on fringe-by-fringe basis, leaving some measurement errors at the joint points between adjacent fringes. As a future work we will investigate the use of multiple triangular fringe patterns with the aim to improve the measurement accuracy.

REFERENCES

[1] Takeda, M., Ina, H. and Kobayashi, S., "Fourier-transform method of fringe-pattern analysis for computer-based topography and interferometry," J. Opt. Soc. Am. 72 (1), 156–160 (1982).

[2] Takeda, M. and Mutoh, K., "Fourier transform profilometry for the automatic measurement of 3-D object shapes," Appl. Opt. 22 (24), 3977–3982(1983).

[3] Su, X. and Chen, W., "Fourier transform profilometry: a review," Opt. Lasers Eng. 35, 263-284(2001).

[4] Zhang, H., Lalor, M.J. and Burton, D.R., "Spatiotemporal phase unwrapping for the measurement of discontinuous objects in dynamic fringe-projection phase-shifting profilometry," Appl. Opt. 38 (16), 3534–3541(1999).

[5] Halioua, M. and Liu, H.C., "Optical three-dimensional sensing by phase measuring profilometry," Opt. Lasers Eng. 11, 185-215(1989).

[6] Li, J., Su, H. and Su, X., "Two-frequency grating used in phase-measuring profilometry," Appl. Opt. 36 (1), 277–280(1997).

[7] Baker, M.J., Chicharo, J.F. and Xi, J., "An Investigation into Temporal Gamma Luminance for Digital Fringe Fourier Transform Profilometers," in IEEE International Symposium on Intelligent Signal Processing, 4447501 (2007).

[8] Baker, M.J., Xi, J. and Chicharo, J.F., "Elimination of γ Non-linear Luminance Effects for Digital Video Projection Phase Measuring Profilometers," in 4th IEEE International Symposium on Electronic Design, Test & Applications, 496-501(2008).

[9] Hu, Y., Xi, J., Li, E., Chicharo, J.F. and Yang, Z., "Three-dimensional profilometry based on shift estimation of projected fringe patterns," Appl. Opt. 45 (4), 678–687(2006).
[10] Hu, Y., Xi, J., Chicharo, J.F., Li, E. and Yang, Z., "Discrete cosine transform based shift estimation for fringe pattern profilometry using generalized analysis model," Appl. Opt. 45 (25), 6560–6567(2006).
[11] Hu, Y., Xi, J., Chicharo, J.F., Cheng, W. and Yang, Z., "Inverse Function Analysis Method for Fringe Pattern Profilometry," IEEE Trans. Instrum. Meas. 58 (9), 3305–3314(2009).
[12] Su, X., Su, L., Li, W. and Xiang, L., "New 3D profilometry based on modulation measurement," Proc. SPIE 3853, 1–7(1998).
[13] Toyooka, S. and Tominga, M., "Spatial fringe scanning for optical phase measurement," Opt. Commun. 51, 68–70(1984).
[14] Toyooka, S. and Iwaasa, Y., "Automatic profilometry of 3-D diffuse objects by spatial phase detection," Appl. Opt. 25 (10), 1630–1633(1986).
[15] Rodriguez-Vera, R. and Servin, M., "Phase locked loop profilometry," Opt. Laser Technol. 26, 393–398(1994).
[16] Meadows, D.M., Johnson, W.O. and Allen, J.B., "Generation of surface contours by moiré patterns," Appl. Opt. 9 (4), 942–947(1970).
[17] Wust, C. and Capson, D.W., "Surface profile measurement using color fringe projection," Mach. Vision Appl. 4, 193–203(1991).
[18] Huang, P., Ho, Q., Jin, F. and Chiang, F., "Colour-enhanced digitial fringe projection technique for high-speed 3-D surface contouring," Opt. Eng. 38 (6), 1065–1071(1999).
[19] Moore, A.J., Mendoza-Santoyo, F., "Phase demodulation in the space domain without a fringe carrier," Opt. Lasers Eng. 23, 319–330(1995).
[20] Villa, J., Servin, M. and Castillo, L., "Profilometry for the measurement of 3-D object shapes based on regularized filters," Opt. Commun. 161, 13–18(1999).
[21] Guo, H., He, H. and Chen, M., "Gamma correction for digital fringe projection profilometry," Appl. Opt. 43(14), 2906-2914(2004).
[22] Zhang, S. and Huang, P.S., "Phase Error Compensation for a 3-D Shape Measurement System Based on the Phase Shifting Method," Opt. Eng. 46 (6), 063601(2007).
[23] Zhang, S. and Yau, S., "Generic nonsinusoidal phase error correction for three-dimensional shape measurement using a digital video projector," Appl. Opt. 46 (1), 36-43(2007).
[24] Pan, B., Kemao, Q., Huang, L. and Asundi, A., "Phase error analysis and compensation for nonsinusoidal waveforms in phase-shifting digital fringe projection profilometry," Opt. Lett. 34(4), 416–418(2009).
[25] Liu, K., Wang, Y., Lau, D.L., Hao, Q. and Hassebrook, L.G., "Gamma model and its analysis for phase measuring profilometry," J. Opt. Soc. Am. 27(3), 553-562(2010).